**Hippocampal sharp wave ripples and coincident cortical ripples orchestrate human semantic networks**

Akash Mishra[1,2], Serdar Akkol[1,3], Elizabeth Espinal[1,4], Noah Markowitz[1], Sabina Gherman[1], Gelana Tostaeva[1], Elisabeth Freund[1], Ashesh D. Mehta[1,2], Stephan Bickel[1,2,5]

[1]The Feinstein Institutes for Medical Research, Northwell Health, Manhasset, NY, United States
[2]Departments of Neurosurgery and Neurology, Zucker School of Medicine at Hofstra/Northwell, Hempstead, NY, United States
[3]Elmezzi Graduate School of Molecular Medicine, Northwell Health, Manhasset, NY, United States
[4]Department of Psychological and Brain Sciences, Drexel University, Philadelphia, PA, United States
[5]Center for Biomedical Imaging and Neuromodulation, Nathan Kline Institute, Orangeburg, NY, United States

**Corresponding authors**:
Akash Mishra (amishra4@northwell.edu) and Stephan Bickel (sbickel@northwell.edu)

## Abstract

Episodic memory function is predicated upon the precise coordination between the hippocampus and widespread cortical regions. However, our understanding of the neural mechanisms involved in this process is incomplete. We utilize human intracranial recordings during a list learning task and demonstrate hippocampal sharp-wave ripple (SWR)-locked reactivation of specific semantic processing regions during free recall. This cortical activation consists of both broadband high frequency (non-oscillatory) and cortical ripple (oscillatory) activity. SWRs and cortical ripples in a major semantic hub, the anterior temporal lobe, co-occur and increase in rate prior to recall. Coincident hippocampal-cortical ripples are associated with a greater increase in cortical reactivation, show specificity in location based on recall content, and are preceded by cortical theta oscillations. These findings may represent a reactivation of hippocampus and cortical semantic regions orchestrated by an interplay between hippocampal SWRs, cortical ripples, and theta oscillations.

## Introduction

Human memory is thought to depend on the intricate bidirectional interplay between the hippocampus and memory-containing cortical regions. The mechanisms by which these distant regions communicate and synchronize activity are of particular interest because they may elucidate the processes that underlie human memory and represent therapeutic targets for the amelioration of memory impairment. Hippocampal sharp-wave ripples (SWRs) are high-frequency (80-140 Hz) oscillations that reflect coordinated neuronal population firing in the hippocampus and are associated with the hippocampal recruitment of cortical regions during memory encoding and recall[1,2]. SWRs likely play a role in a two-stage framework of memory where information is initially encoded in the hippocampus and consolidated in the cortex, and during memory retrieval, the hippocampus reactivates these memory-containing cortical sites[3–10]. In support of this theory, studies have demonstrated SWR-locked reactivation of specific memory-containing cortical regions through increases of high frequency activity (HFA, 70-150 Hz) during encoding and recall[7,8,11–13]. Intriguingly, more recent studies identified ripple-like oscillatory phenomena in cortical regions (“cortical ripples”) that are temporally-coincident with SWR, similar in morphology (frequency and duration) as SWR, and associated with improved memory performance[9,14–19]. However, the function and importance of these phenomena to memory performance remain unclear. This includes whether SWR-coincident cortical ripples show specificity for region or content and how oscillatory cortical ripples differ from non-oscillatory increases in the high frequency band (broadband high frequency activity, or BHA), which is associated with neuronal population activation[20–22]. Finally, as coincident ripples reflect periods of heightened hippocampal-cortical binding[15], there is a potential overlap in function between human ripple oscillations and theta oscillations. A potential relationship between ripple and theta oscillations has been proposed in human NREM sleep[23], but this remains to be further explored in the awake, task state.

Semantic processing networks are activated during speech perception and display precise coordination across widespread cortical regions[24–27]. This represents the activation of an intricate hierarchical processing ensemble, initiated in the primary auditory cortex and advancing to cortical regions. This exists on an ascending gradient where the level of comprehension and complexity increases as higher-order regions are recruited (e.g. syllables to words to sentences)[28–30]. Recent study has identified a significant contribution to semantic processing from a large, distributed cortical network that involves frontal, anterior and posterior temporal, and parietal regions[26,27,31]. Further, the anterior temporal lobe (ATL) may serve as a critical node in this network, as it coordinates semantic processing[32–35] and serves as the interface between the posterior temporal lexical-semantic areas and frontal cortex regions[36]. This warrants the investigation of whether SWRs show specific, functional interaction with this network during word list memory encoding and retrieval.

We use an auditory word list and sentence learning task with delayed verbal free recall to examine the relationship between ripples (both SWR and cortical ripples) and the activation of semantic networks during encoding and recall. We recorded intracranial electroencephalography (iEEG) from individuals undergoing invasive neuromonitoring for the treatment of intractable epilepsy to gain rare neural recordings of semantic and memory networks with high spatial and temporal resolution. We show that SWRs are associated with the activation of specific cortical semantic network regions, including both BHA and cortical ripples. Further, coincident SWR-ATL cortical ripple oscillations are preceded by ATL cortical theta oscillations. These results extend our understanding of the function of SWRs to the dynamic activation of semantic networks and further elucidate the mechanisms by which SWRs and cortical ripples coordinate the hippocampal-neocortical memory network.

## Results

### Behavioral results

Nine participants participated in a word list learning task with verbal free recall (Figure 1A; Figure S1). On average, subjects recalled 4.1±2.0 words (of 12 total) per trial across 1.6±0.8 recall events (defined as recall onsets with an inter-response interval exceeding 4 seconds) per trial (median recall duration was 2.4 seconds). Participants showed a trend towards an increased number of words recalled in trials where words were assembled into sentences (sentence condition) compared to when they were not (non-sentence condition) (Z=1.953, p=0.051).

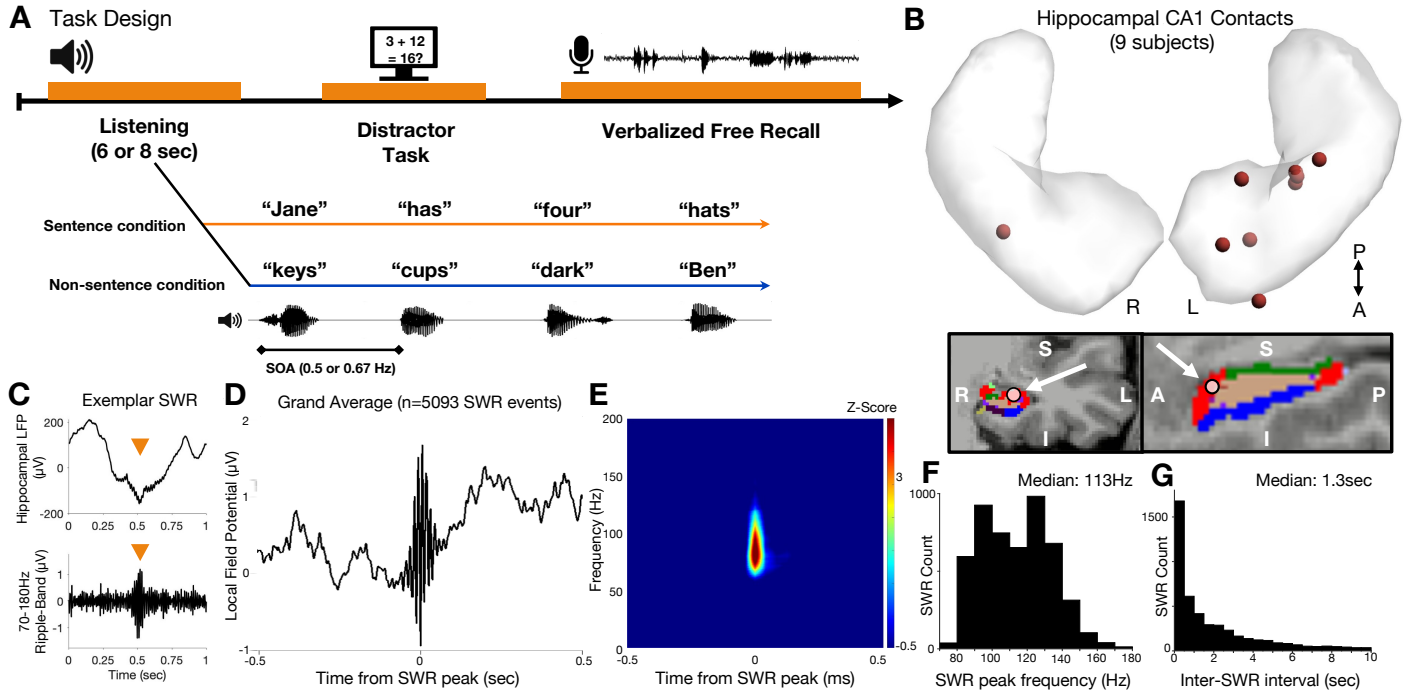


Figure 1. Experimental design and hippocampal sharp wave ripple detection. (A) Experimental design and example stimuli presented to subjects. subjects listen to a list of twelve words assembled into either 3 sentences (of 4 words each) or a randomized word list. Then, after an arithmetic distractor task, subjects were asked to freely recall as many words as possible. Sentence and non-sentence trials were randomized and interleaved for a total of 30 trials. (B) (Top) Hippocampal depth electrode selection across all subjects. One point represents an individual subject. (Bottom) Representative structural reconstruction of hippocampal depth electrodes in one patient in coronal (left) and sagittal (right) views; white arrows denote CA1 recording site implemented for SWR detection analysis. Red parcellation indicates CA1 subregion. (See Figure S2 for similar reconstructions for other subjects). (C) Example of SWRs as they appear in (*top*) the raw hippocampal local field potential and (*bottom*) the 70-180 Hz ripple-band. (D) Grand average peri-SWR field potential locked to SWR peak for n=5093 SWRs from 9 subjects. (E) Wavelet spectrogram locked to SWR peak for n=885 SWRs from one representative patient. Warmer colors indicate a higher spectral power in that frequency-time combination. (F) Distribution of SWR peak frequencies and (G) inter-SWR interval for all n=5093 SWRs.

**SWR rate is modulated by encoding of word lists and subsequent free recall**

We identified SWRs from the local field potentials (LFPs) of hippocampal contacts located within (or as close as possible to) the CA1 subfield (Figure 1B; Figure S2), referenced to the closest white-matter contact 8.8mm away. Across 9 subjects, we identified 5093 SWRs during all task periods (encoding, distractor, and recall). The SWR-locked LFP across all SWRs is depicted in Figure 1D. The spectral decomposition for 885 SWRs from one subject is depicted in Figure 1E. The median peak SWR frequency across all subjects was 113Hz (Figure 1F) and the median inter-SWR interval duration was 1.3sec (Figure 1G). These findings align with prior human SWR studies[8,37–39].

Since SWRs play a role in both encoding and recall[1], we next investigated the SWR rate during these task periods. We created peri-event time histograms (PETHs) of SWRs during the list presentation (n=7 subjects) (Figure 2A). Two subjects were excluded from this analysis because they recieved a different presentation inter-stimulus interval (500ms instead of 667ms; the PETH for these subjects is shown in Figure S3). After removal of 33 trials where external interruption or misclick occurred, we assessed 177 word presentation trials (8-second word list presentation, followed by a 2-second rest period). The SWR rate was significantly increased starting 1400 ms after list presentation onset and decreased 800ms after presentation offset ($p<0.001$, permutation test) (Figure 2A). SWR rate did not significantly differ for presentation of sentence and non-sentence word lists (Figure S4). Next, we assessed SWR dynamics during memory retrieval by assessing a PETH locked to verbal free recall onsets. SWR rate was significantly increased 1000ms prior to recall onset (n=342 trials; $p=0.037$, permutation test) (Figure 2B). Importantly, SWR rate was not reliably modulated by random vocalizations captured during the task period[8] (Figure S5).

As SWRs represent a potential marker for effective memory processes, increased SWR rates during memory encoding and recall may be associated with improved memory performance. To assess this, we performed a median split of the total number of recalled words per trial and identified trials where subjects executed a good response (number of words recalled in the trial exceeds the patient's median across all trials) or poor response (below or equal to the median). Across subjects, the mean number of words recalled during a good recall was 5.7±1.8 words (139 events) compared to 3.2±1.4 for poor recalls (203 events). We then compared SWR dynamics prior to recall onset for good and poor recalls. SWR rate was higher for trials that resulted in a good recall in the 1000ms window prior to verbal free recall compared to poor recalls ($p=0.0314$, permutation test) (Figure 2C). Next, we compared SWR rate during word list presentation (one rate value per subject) for trials where subjects subsequently provided a good versus poor response. SWR rate during the word list presentation period was higher for trials where subjects subsequently executed a good recall (0.222 SWR/second) compared to poor recall (0.167 SWR/second) (two-tailed Mann-Whitney $U=109$, $n1=n2=9$, $p=0.0379$) (Figure 2D). This group-level relationship holds a trend when assessing SWR rate in the window around free recall onset (-2 to +0.5 seconds relative to free recall onset; two-tailed Mann-Whitney $U=39$, $n1=n2=9$, $p=0.0547$) (Figure 2E). Taken together, SWRs may reflect memory network activity during encoding and retrieval of word lists.

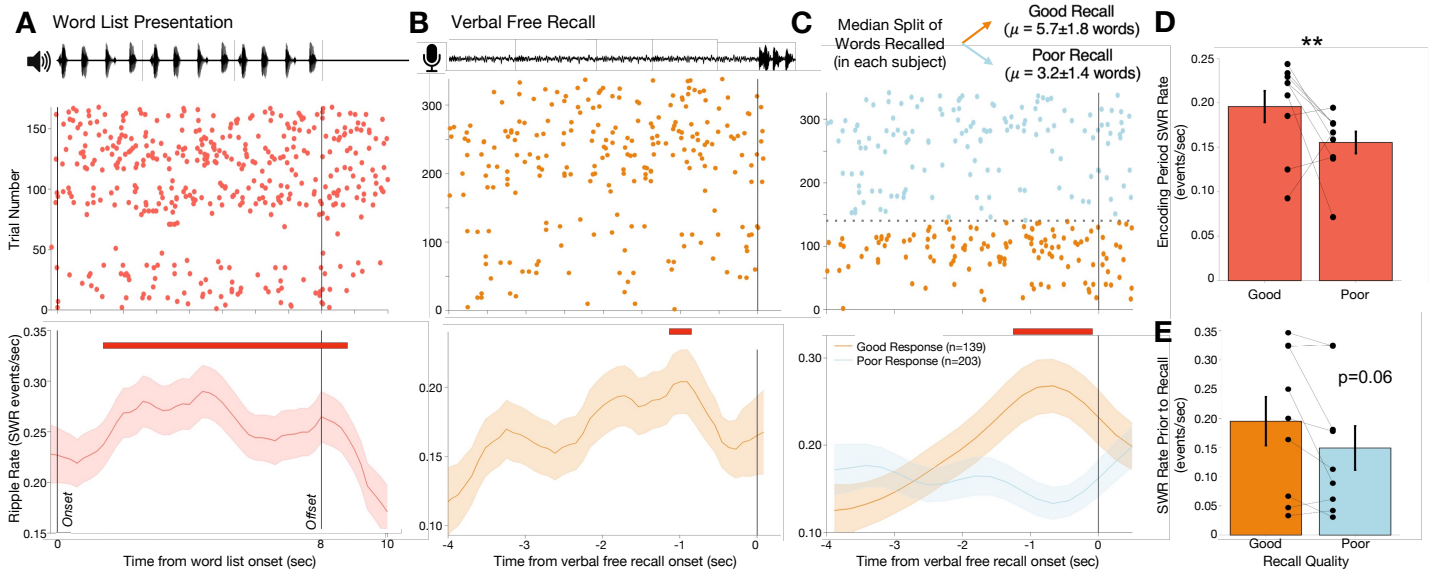


**Figure 2**. Sharp-wave ripple dynamics during word list presentation and free recall. (A) SWR raster plot and peri-event time histogram (PETH) time-locked to the onset of word list presentation (n=168 trials across 7 subjects), depicting a sustained increase in SWR rate in response to word list presentation compared to baseline that subsequently diminishes after offset of word presentation (vertical line). Two subjects were removed from this analysis due to variation in word presentation frequency but demonstrated a similar SWR increase (Figure S3). Red line indicates significance at p<0.05 (permutation test compared to shuffled SWR times in the 2-second post-trial resting period). Shaded areas represent one bootstrap standard error computed over SWR events. (B) SWR raster plot and PETH time-locked to the onset of distinct recall vocalizations (n=338 trials across 9 subjects), indicating a transient response-locked increase in SWR rate. Red line indicates significance at p<0.05 (permutation test shuffling SWR times across this PETH epoch). Shaded areas represent one bootstrap standard error computed over SWR events. (C) SWR raster plot and PETH time-locked to onset of distinct recall vocalizations. Data is median split by the number of words recalled during that trial where "good response" (n=139 trials) was a trial where the patient recalled more than their median number of recalled words across trials and a "poor response" was equal to or below the median (n=203 trials). Red line denotes significance at p<0.05 (cluster-based permutation test clustering across time, p<0.05). Shaded areas represent one bootstrap standard error computed over SWR events. (D) Bar graph of mean SWR rate during the encoding phase for trials that contained a good response and poor response. Each point represents the mean SWR rate per subject and lines connect data for each subject. Error bar depicts standard deviation across subjects. Stars denote significance at p<0.05 (Mann-Whitney U). (E) Bar graph of mean SWR rate during the two second window prior to onset of verbal free recall in trials that contained a good response and poor response. Each point represents the mean SWR rate per subject and lines connect data for each subject. Error bar depicts standard deviation across subjects.

## SWR reactivate functional semantic network regions during free recall

SWRs are thought to facilitate the communication between the hippocampus and specific cortical regions[1]. Hence, SWRs during the recall portion of a word list learning task may activate cortical regions that were initially engaged during word list encoding. We first defined cortical semantic networks by examining HFA during word list presentation in all cortical contacts (Figure S1), similar to a recent human iEEG study[31]. We identified 150 contacts that exhibited higher HFA during the listening of sentence compared to non-sentence word lists ("sentence-responsive") and 79 cortical contacts that showed higher HFA for the opposite ("non-sentence-responsive") (FDR-corrected p<0.01, permutation test). Figure S6 depicts the difference in HFA activation between preferred and non-preferred trials across all contacts. Identified contacts were distributed across several higher-order cortical regions. As a control, we also identified an additional 57 cortical contacts that were responsive to both sentence and non-sentence trials (p<0.01, one-sample t-test) (Figure 3A).

We then assessed the interaction between SWR in the recall periods and this semantic network. We observed a significant peri-SWR HFA increase in cortical contacts when there was congruence between the electrode preference and trial type ("preferred" trial-electrode combination) compared to when there was no congruence ("non-preferred" combination) (p=0.031, cluster-based permutation test) (Figure 3C). This effect is also readily visible on the single contact level (sentence-responsive contact: n=180 words in sentence list, n=168 words in non-sentence list; two-sample t(346)=3.016, p=0.027; reactivation: cluster-based permutation test clustering timebins, p=0.018) (Figure 3B). To further evaluate the regional distribution of this effect, we calculated the effect size of SWR-locked HFA reactivation between preferred and nonpreferred trials in a 500ms peri-SWR window (Figure 3D; also visualized in the spectrograms in Figure S8). Temporal lobe contacts displayed the highest difference between preferred and non-preferred SWR-locked reactivation (Figure S9).

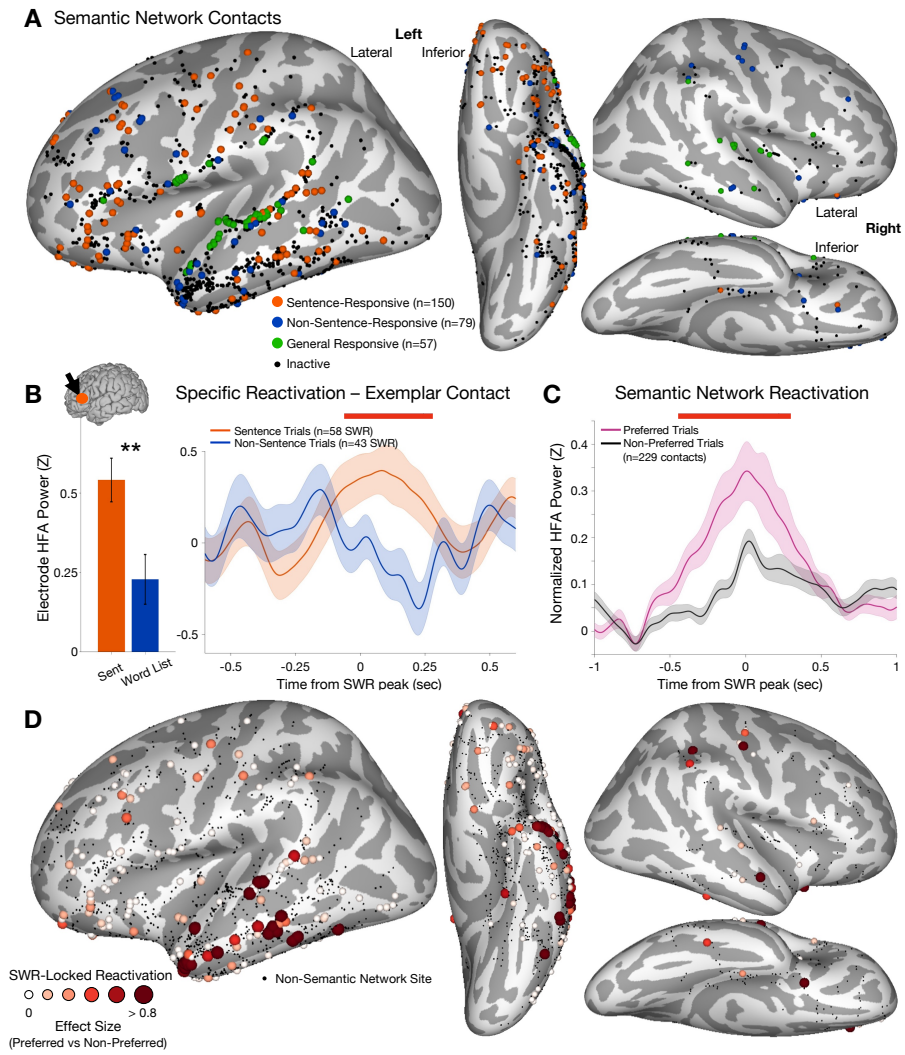


**Figure 3.** Sharp wave ripple-locked reactivation of the semantic network. (A) Left lateral *(left)*, left inferior *(middle)*, right lateral *(right upper)*, and right inferior *(right lower)* views on inflated brains of locations of sentence-responsive (blue, n=150), non-sentence-responsive (blue, n=79), and general semantic-responsive (green, n=57) contacts on an inflated brain. (Also see increase in HFA during preferential word list presentation in Figure S6.) (B) Peri-SWR HFA responses in an exemplar electrode. *(Left)* HFA response during word presentation by sentence and non-sentence trial (n=15 trials and n=180 words each, error bars denote standard deviation across trials, stars denote significance at p<0.05, two-sample t-test), *(inset)* location of the selected electrode, *(right)* HFA response locked to SWR that occurred in the recall period when subjects recalled words from either sentence (n=58 SWR) or non-sentence trials (n=43 SWR). Red bar represents significant time bins at p<0.05 (cluster-based permutation test clustering across time). Shaded areas represent one standard error computed over SWR events. (C) HFA time-locked to peak of SWR events that occurred during recall of trials that aligned with the contact's preference as compared to when they did not. Red line denotes significant time bins at p<0.05 (cluster-based permutation test, n=212 electrode pairs). Shaded areas represent one standard error computed across contacts. (Also see spectrogram of this analysis in Figure S8.) (D) Reactivation effect size (in Cohen's d) for semantic network contacts (combining sentence-responsive and non-sentence-responsive contacts) comparing peri-SWR HFA reactivation during the recall period of preferred versus non-preferred trials. Darker colors and larger electrode sizes depict larger effect sizes.

## SWR-Associated ATL HFA: Coincident Cortical Ripple or BHA?

A region of prominent HFA activation in our study was the ATL (Figure 3D). This is in line with prior studies[9,13,40] that show hippocampal-cortical coupled ripples in a word association task in this region. We aimed to replicate these findings using our list learning task and extend them by further investigating the potential relationship between non-oscillatory (BHA) and oscillatory (cortical ripple) activity in the ATL.

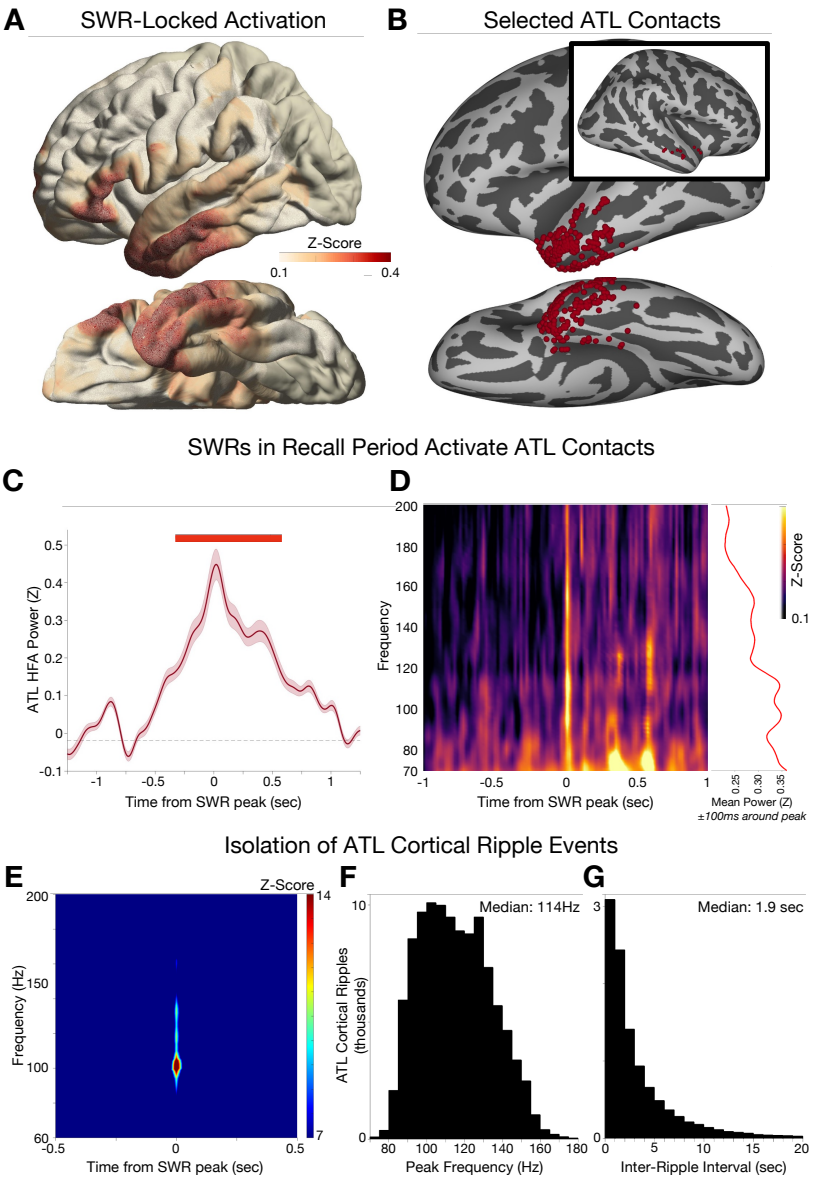


**Figure 4.** Properties of anterior temporal lobe cortical ripples. (A) Left lateral *(top)* and left inferior *(bottom)* views of normalized brains with overlaid heatmap representing regions of increased HFA increase locked to peaks of SWR within the recall period across all contacts. Darker colors represent increased HFA, and uncolored regions represent no electrode coverage in the region. (B) Left lateral *(top)*, left inferior *(bottom)*, and right lateral *(inset)* views on inflated brains depicting the location of n=196 anterior temporal lobe contacts across subjects. Contacts were selected on patient-specific imaging and precise location may be distorted in the transfer to standardized space. (C) HFA increase locked to peaks of SWR within the recall period for n=196 ATL contacts. Red line denotes significant timebins at $p<0.05$ (cluster-based permutation test against pre-SWR baseline). Shaded areas represent one standard error computed across ATL contacts. (D) *(Left)* Wavelet spectrogram of ATL high frequency power locked to SWRs alongside *(Right)* mean power in the 40ms window centered around SWR peak for each frequency represented in the spectrogram depicting an increase in the 90-120 Hz range. Hotter colors represent increased power. (E) Wavelet spectrogram time locked to ATL cortical ripple peak (n=7773 events from one representative patient with n=12 ATL contacts). Warmer colors indicate a higher spectral power in that frequency-time combination. (F) Distribution of peak frequencies and (G) and inter-ripple duration for all detected ATL cortical ripples (n=108510 events in n=196 contacts, n=9 subjects).

We first assessed HFA increases locked to SWRs in the recall period (500ms window centered on SWR peak) across all cortical contacts (Figure 4A, also visualized in effect size analysis for all cortical contacts in Figure S9) and identified an increase in the area corresponding to the ATL. To investigate this further, we isolated ATL contacts (n=218) using anatomical reference and excluded 22 contacts that overlapped with the functionally-defined semantic network (Figure 4B). Not surprisingly, SWRs were associated with a significant increase in ATL HFA ($p<0.001$, cluster-based permutation test) (Figure 4C), maximally at the time of the SWR peak. Spectral analysis of this activity showed a spectral peak in the 80-120 Hz range as well as an increased BHA (Figure 4D). Since the spectral peak was found at the expected frequency range of cortical ripples, we conducted a ripple detection analysis for all ATL contacts. Across all ATL contacts, cortical ripples occurred with peak frequencies

predominantly within the 80-140 Hz range (Figure 4E) but centered around 114 Hz (Figure 4F) and with a median inter-ATL cortical ripple interval of 1.9 seconds (Figure 4G).

We next assessed the synchronicity of ripple oscillations by computing a cross-correlogram between all SWRs during the recall period and ATL cortical ripples. There was significant coincidence ($p<0.01$, permutation test), with a mean delay of cortical ripple peak relative to SWR peak of 14ms (Figure 5A). Further, the proportion of SWRs that were associated with an ATL cortical ripple increased 700ms prior to verbal free recall and was sustained until recall onset ($p=0.0354$, permutation test) (Figure 5B). Thus, SWRs increase in the one-second window prior to recall (Figure 2B) and these SWRs are more likely to co-occur with ATL cortical ripples. Interestingly, compared to non-coincident ATL cortical ripples, coincident ATL cortical ripples in the recall period were of higher frequency (median 119 Hz compared to 113 Hz; $z=5.868$, $p<0.001$) and shorter duration (80ms compared to 96ms; $z=7.665$, $p<0.001$) (Figure S10).

The presence of cortical ripples raises an important methodological question: are SWR-locked increases in HFA a product of synchronous ATL cortical ripples, non-oscillatory neuronal population firing (BHA), or a combination of both? To this end, ATL cortical ripples during the recall period that were coincident with an SWR exhibited a greater increase in associated HFA compared to those not coincident with an SWR ($p<0.001$, cluster-based permutation test) (Figure 5C). Both coincident and non-coincident ATL ripples exhibited a significant increase in ripple-band power (especially between 80-140 Hz), but only coincident ATL cortical ripples exhibited a significant increase in high frequency activity above 140 Hz ($p=0.032$, cluster-based permutation test) (Figure 5D, also depicted in the spectral plots in Figure S11). This is indicative of non-oscillatory BHA that is more associated with SWR-coincident ATL cortical ripples.

**Coincident Hippocampal-Cortical Ripples Across the Semantic Network**

Coincident ripple oscillations may serve as a precise mechanism for synchronizing the activity of multiple nodes within the hippocampal-cortical memory network. Hence, we examined the impact of coincident ripples on the recruitment of cortical regions, with an emphasis on elucidating the dynamics of SWR, cortical ripples in the ATL, and cortical ripples across the semantic network (functionally-defined; combining sentence-responsive and non-sentence responsive contacts). First, SWRs that were coincident with ATL ripples during the recall period exhibited a greater increase in HFA across all contacts in the semantic network (n=491 coincident hippocampal-ATL ripples, n=276 non-coincident SWRs) ($p<0.001$, cluster-based permutation test) (Figure 5E). This may indicate that coincident hippocampal-ATL ripples more optimally recruit the cortical semantic network. However, the same caveat as above applies: this may be a product of cortical ripples in the semantic network that co-occur with SWR.

To investigate this possibility, we identified cortical ripple events in the semantic network contacts, and repeated the same analysis as in Figure 5E but removed all SWR events where there was a coincident semantic network cortical ripple (that is, we assessed the semantic network activation by SWR that were and were not coincident with an ATL cortical ripple after removing all SWR that contained a semantic network ripple event). We no longer found a significant semantic network HFA increase resulting from coincident hippocampal-ATL ripples ($p=0.293$, cluster-based permutation test; n=157 SWRs where SWR-ATL coincident ripples occurred and n=147 events where SWR did not co-occur with an ATL cortical ripple) (Figure 5F). Hence, it is probable that the witnessed effect of coincident hippocampal-ATL ripples on semantic network HFA is influenced by coincident semantic network cortical ripples.

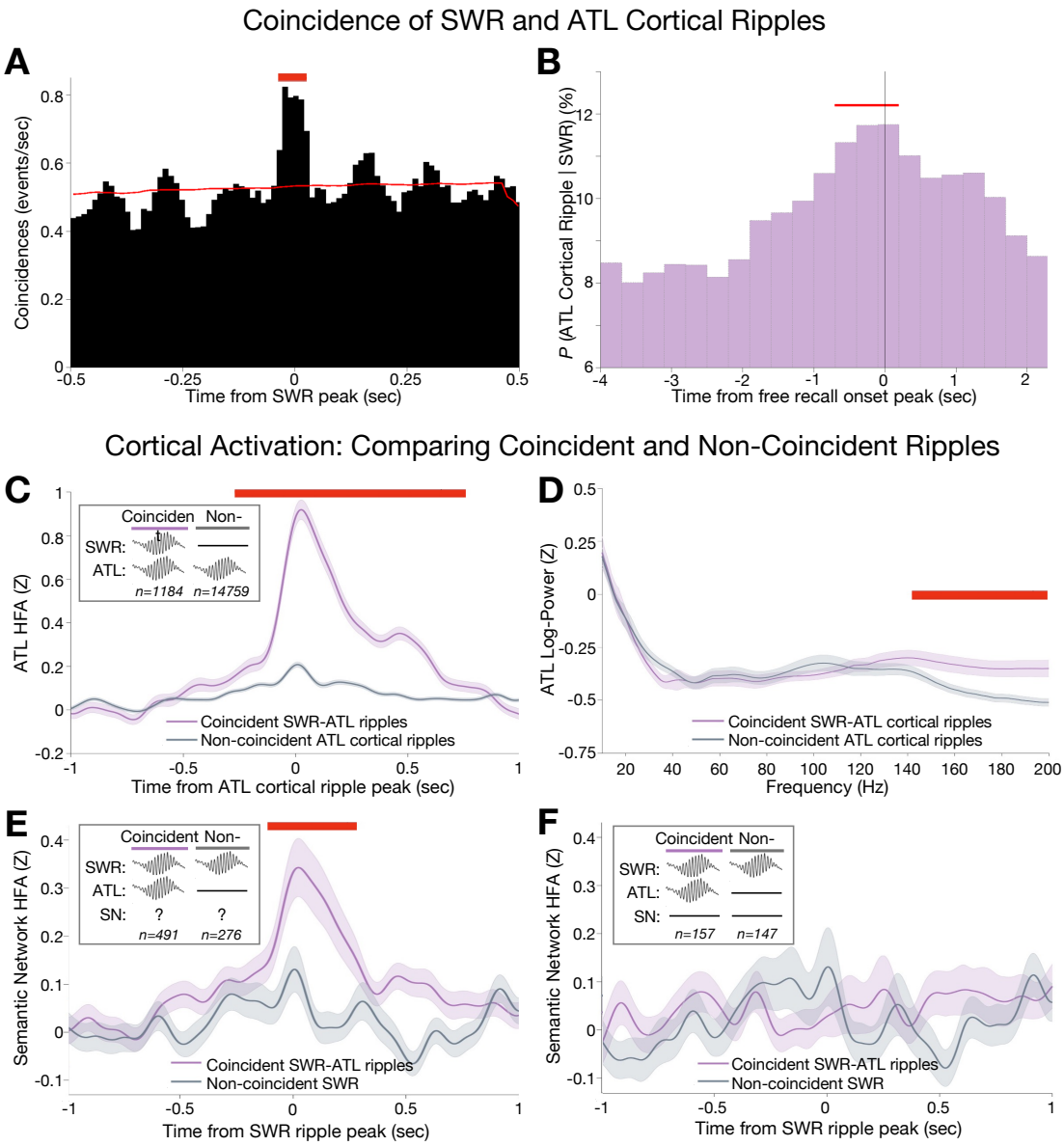


**Figure 5.** Ripples and ripple-locked activity across the hippocampus, anterior temporal lobe, and other semantic areas. (A) Cross-correlograms between ATL cortical ripples (n=15943 across n=196 ATL contacts) and SWRs (n=772 across n=9 hippocampal contacts) within the recall period across n=9 subjects. Red line denotes significant time bins at p<0.05 (permutation test with jittered cortical ripple timing), indicating high coincidence. (B) Joint probability of coincident SWR and ATL cortical ripple as a function of time relative to verbal recall onset. Red line denotes significant time bins at p<0.05 (permutation test with jittered cortical ripple timing). A significant increase is visualized within one second window prior to verbal recall onset. (C) ATL HFA locked to peak of ATL cortical ripples in the recall period separated by whether the ATL cortical ripple was coincident with an SWR (n=1184) or not (n=14759). Red line denotes significant time bins at p<0.05 (cluster-based permutation test). Shaded area represents standard error computed across ripple events. (See spectral profile of this difference in Figure S11.) (D) High frequency spectral profile of ATL cortical ripples in the recall period that were associated with SWRs coincident with compared to not coincident with SWRs. Red line denotes significant frequencies at p<0.05 (cluster-based permutation test). Shaded area represents one standard error computed across ripple events. (E) HFA in semantic network contacts locked to peaks of SWR in the recall period by whether the SWRs was associated with an ATL cortical ripple (n=491) or not associated (n=276). Red line denotes significant time bins at p<0.05 (cluster-based permutation test). Shaded areas represent one standard error computed across ripple events. (F) Same as in (E) but remove all SWRs epochs containing a coincident cortical ripple within the semantic network removed. Shaded areas represent one standard error computed across ripple events.

We then investigated whether semantic network cortical ripples show any spatial specificity during recall of specific items. We assessed whether there was an increased coincidence of ripples for trials where the SWRs and semantic network contact showed congruence in preference (i.e. a SWR that occurred prior to free recall within a sentence trial and coincident ripple occurring in a sentence-responsive contact, and the same for non-sentence trials/contacts) compared to when there was no congruence (i.e. SWR in a sentence trial and cortical ripples in a contact that had preference for non-

sentence trials, or vice versa). The rate of triple co-occurrence of ripples in the hippocampus, ATL, and semantic network contact was increased when there was congruent preference compared to when there was no congruence (2.1% of hippocampal-ATL-cortical contact pairs showed coincidence for congruent preference compared to 1.9% of pairs showing coincidence for non-congruent preference, $X^2(1, n=346182)=18.802$, $p<0.001$). This is indicative of content-dependent spatial specificity of cortical ripples.

**Coincident SWR-cortical ripples are associated with cortical low theta oscillations**

Thus far, this analysis has probed the relationship between ripples and HFA/BHA, but a key missing element is the relationship to lower frequencies. Qualitatively, a possible theta modulation of the hippocampal-ATL ripple coincidence is already notable in Figure 5A. Indeed, coincident SWR-ATL ripples (n=1184) were associated with a significant increase in ATL low theta power (3-5 Hz) compared to non-coincident ATL ripples (n=14759), (p=0.016, permutation test) (Figure 6A). The time course of the theta power increase shows that it is roughly coincident with the ATL cortical ripple peak (p=0.003, permutation test) (inset, Figure 6A). To confirm the presence of theta oscillations in single trials around the coincident ATL ripples, we utilized the FOOOF toolbox[42]. Detected theta oscillations showed a peak frequency between 3-5 Hz (Figure 6B). Finally, to determine the temporal relationship between coincident hippocampal-cortical ripple oscillations and theta oscillations, we constructed a cross-correlogram between detected theta oscillation peaks and the peaks of ATL cortical ripples that were and were not coincident with SWR. ATL cortical ripples that were coincident with SWR co-occurred with ATL theta oscillations at a significantly higher rate than non-coincident ATL cortical ripples (p=0.002, cluster-based permutation test) (Figure 6C). The theta oscillation peak is, on average, delayed by 109ms relative to the coincident hippocampal-ATL ripple peak. This is suggestive of a potential relationship between synchronous hippocampal-ATL ripples and ATL theta oscillations.

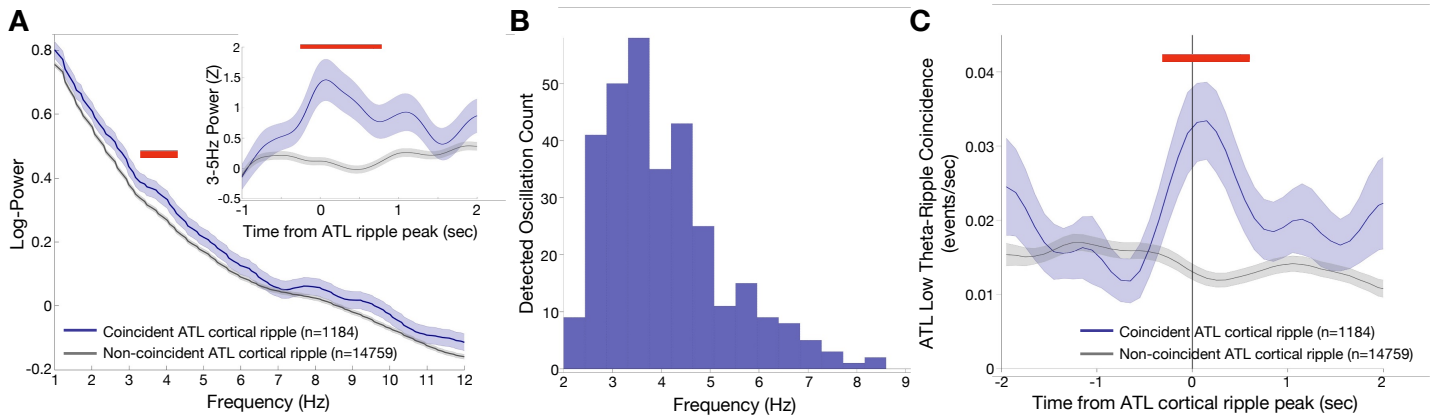


**Figure 6.** Relationship between cortical ripples and theta oscillations. (A) Low frequency spectral profile of ATL activity locked to peak of ATL cortical ripple that were coincident with a SWRs (n=1184) and not coincident with SWRs (n=14759). Red line denotes significant frequencies at p<0.05 (cluster-based permutation test). Shaded areas represent one standard error across ripple events. *(Inset)* Power in the 3-5 Hz low theta frequency range across time when locked to peak of ATL cortical ripples occurring in the recall period. Red line denotes significant time bins at p<0.05 (cluster-based permutation test). Shaded areas represent one standard error across ripple events. (B) Distribution of peak frequency of detected low frequency oscillations around ATL cortical ripples that were coincident with a SWR. (C) Cross-correlograms between peak of ATL cortical ripples that were coincident with SWR during the recall period and peak of ATL theta oscillations. Red line denotes significant time bins at p<0.05 (cluster-based permutation test). Theta oscillations occurred at a peak lag of 109 ms relative to coincident ATL cortical ripples. Shaded areas represent one standard error computed across cortical theta peak events.

## Discussion

Memory formation and retrieval is a complex process that involves coordination of the hippocampus and cortical regions. Neural oscillations are a candidate mechanism that may support this cross-regional synchronization. We used the rare clinical opportunity to attain direct, in-vivo intracranial recordings from the human hippocampus and widespread cortical regions during a word list learning task. We show that the hippocampal SWR rate increases during encoding and recall, and the magnitude of increase correlates with recall performance. During memory retrieval, SWRs exhibit content-dependent reactivation of specific cortical regions that exhibit selective activity during word list perception. In a major semantic hub, the ATL, SWRs during retrieval are associated with both oscillatory (co-incident cortical ripples) and non-oscillatory (BHA) cortical activity. Finally, coincident hippocampal-ATL ripple oscillations are more likely to be associated with cortical theta oscillations. Taken together, we replicate prior findings indicating a function of SWR in the encoding and retrieval of word lists and sentences[11,43], support congruence in the function and mechanisms of SWR across memory tasks in the awake humans[7–9,15,44], and extend our knowledge of the mechanisms and functions underlying cortical ripple oscillations[9,15,16].

### SWR rates during perception predicts memory

The orchestration of memory encoding and retrieval is thought to involve a bidirectional interplay between the hippocampus and memory-containing neocortical regions[45]. A candidate mechanism proposed to underlie this hippocampal-cortical synchronization during encoding and retrieval are hippocampal SWRs. During encoding, these highly synchronized patterns of neuronal firing may bind neuronal activity across regions and strengthen connections, and during recall, they may facilitate the reactivation of the same neuronal firing patterns that were active during encoding[1,46–48]. In both encoding and recall, it is possible that ripples engage multiple specific memory-containing cortical regions[15]. Hence, when the rate of SWRs increases during encoding, there may be increased binding of hippocampal-neocortical activity that strengthens the memory representation. During retrieval, as SWRs function to reactivate memory-containing cortical regions, increased SWR rate may indicate heightened reactivation of relevant memory traces. This would manifest as an increase in SWR rate prior to the onset of free recall, as memory retrieval precedes verbal recall. These increases in SWR rate during successful encoding and retrieval have been identified previously in awake humans[7–9,11,49]. Our findings align with these studies, as we show that SWR rate increases during both word list presentation and free recall. Further, for trials when there is increased recall content (more words recalled), SWR rate is higher during both encoding and recall.

### SWR-locked cortical activity

High frequency activity (HFA) is one method by which the cortical activity associated with SWR may be assessed. It is the part of the iEEG signal that best correlates with neural population spiking[50,51], although it is also generated by high frequency dendritic events in the superficial cortical layers[41]. This method has been utilized previously to identify SWR-associated activity in visual processing regions[8], the default node network[7], and in sleep states, more dispersed cortical networks[10,12]. In our study, we examined if this link between SWR and cortical activations extends to the semantic network.

The auditory presentation of a set of words engages an assembly of interconnected cortical nodes from lower-order primary auditory cortical regions to higher-order regions involved in extracting rich semantic information from its acoustic input[27,31]. To functionally determine the active semantic networks during our task, we identified sentence-preferred and non-sentence-preferred contacts based on their activity during encoding. These contacts were found to be present in widespread frontal and temporal cortical regions, similar to prior studies using a similar approach[25,27,31]. During recall, we find increased cortical HFA around the SWRs when the content of the recall aligns with the

functional preference of the contact. This finding supports the extension of our knowledge of SWR-associated cortical activation during recall into the language domain. It is interesting to note that the increase in HFA begins 400ms prior to the SWR peak. This may support the hypothesis that during memory recall, the cortex functions to bias hippocampal activity to generate SWR, which then reciprocally activate specific cortical memory representations[4–6,45,48,52,53]. Further study is required to confirm this hypothesis in humans, which may utilize single-unit recordings to achieve more granular resolution of neuronal activity.

**Coincident ripple oscillations**

Next, we expanded our analysis beyond this functionally-defined semantic network to the ATL. This was motivated by recent human word association studies proposing a role of SWR in the reactivation of specific neuronal assemblies in this region[40]. Additionally, the ATL was one of the most activated areas in our data-driven SWR-locked cortical HFA analysis (Figure 4A; Figure S9). While the exact function of the ATL is still mostly unknown, the hub-and-spoke theory suggests that this region is thought to coordinate the activation of individual semantic processing nodes to effectively retrieve higher-order semantic concepts[54,55]. This aligns with clinical outcomes showing that patients with anterior temporal lobectomies of the dominant cortex have increased risk of postoperative naming deficits[56–58]. As expected, we find that, during the recall period, SWR are associated with significant coincident increases in ATL HFA. Interestingly, this increase consists of both BHA and a spectral peak in the frequency range of previously-reported cortical ripples. Cortical ripples are often temporally-coincident with SWRs and may play a key function in rodent[19] and human memory[9,15,19]. These events may signify the precise binding of SWR and cortical activity, reflecting precise reinstatement of cortical memory representations[15,16]. In support of this hypothesis in the domain of verbal memory, studies have utilized a word association task to demonstrate the coincidence of temporal cortex ripples with SWR and illustrate that cortical ripples contain specific neuronal firing patterns indicative of memory representation activation[9,13,40]. This finding partially parallels rodent studies that demonstrate SWR-coincident cortical ripples in association cortices[19]. More recent studies have found this phenomenon to be more ubiquitous across the human cortex, with specific hippocampal-cortical ripple assemblies reactivated during memory retrieval[15,16].

In our study, we find cortical ripples in the ATL, with 7.4% of them showing coincidence with SWRs in the recall period. A rodent study found 20% of association cortex ripples coincident with a SWR[19]. Thus, our identified rate of SWR and coincident cortical ripples is low but similar. There may be several factors that drive this scarcity: (1) poor proximity of contacts to optimal ripple-generating nodes[59]; (2) suboptimal detection of SWR and cortical ripples[37]; and/or (3) recall events may not require coordination of hippocampal-cortical networks[60], or 4) it is possible that the co-ripple rate is lower in humans compared to rodents. In terms of ripple features, cortical ripples are of similar duration and frequency compared to SWRs. However, ATL cortical ripples that co-occur with SWR are of higher frequency and shorter duration compared to cortical ripples that are not coincident with SWR. We speculate that this may be due to different subtypes of cortical ripples. Long-duration ripples are most associated with improved memory consolidation[6,61,62], but shorter-duration ripples may contain more succinct neuronal firing that communicate smaller packets of information. It is also possible that inter-areal communication via coincident ripples requires heightened similarity in frequency and/or duration. To add to this, we find that SWR-ATL cortical ripple coincidence increases prior to recall, even when the increase in SWR is taken into account. Hence, ATL cortical ripples are not exclusive to periods of SWR but their coincidence increases in memory retrieval periods. Next, coincident hippocampal-cortical ripples are more likely to occur in regions that were previously engaged during content encoding, indicating that the content of recall influences the presence of cortical ripples in the semantic network. These findings are suggestive of cortical ripple oscillation networks that exist independently of SWRs but, in times where more optimal hippocampal-cortical synchrony is required, coincidence of SWR and cortical ripples occurs[15].

To summarize, coincident hippocampal-cortical ripple oscillations display unique characteristics that may be evidence of heightened memory network activity, including increased cortical HFA and cortical theta oscillations. Interestingly, in our study, we did not find heightened theta power in the hippocampus associated with coincident ripples. This may warrant further investigation as to whether this was due to methodological shortcomings or if potentially different properties of theta (e.g. phase) show higher association with coincident ripples. One critical piece of this puzzle that is still missing is the directionality or causality of this relationship. Intriguingly, it is possible that the hippocampus itself is not the primary (or "driving") oscillator. This "cortical-centric" approach strays from prior human ripple oscillation studies, which have predominantly focused on hippocampal SWR. This may also point towards a more general function of cortical ripples in human cognition outside of memory.

**Oscillatory and non-oscillatory HFA changes**

The human SWR literature contains reference to both non-oscillatory (BHA)[7,8] and oscillatory (cortical ripple) cortical activity[9,15,16] associated with SWR during memory recall periods. In this study, we investigated the possibility of a co-occurrence between these two phenomena. We show that, when ATL cortical ripples are coincident with SWR, there is a broadband increase in high frequency activity, indicative of heightened non-oscillatory neuronal activity in the ATL. This feature is less prominent for cortical ripples not associated with a SWR. This is in addition to the SWR-coincident ATL cortical ripple oscillations. Hence, SWR are associated with both oscillatory and non-oscillatory cortical activity, and it is possible that these mechanisms function in concert to reflect periods of heightened hippocampal-cortical network activation.

It is interesting that cortical ripples in the semantic network, unlike the ATL, do not display an increase in BHA. This may be partially explained by the relationship between cortical ripples and backbone spiking sequences[13,40,63]. These cortical sequences reflect activation of cortical assemblies where small variation in similar sequences alters the content that is retrieved. Cortical ripples may re-engage the same assemblies but elicit slight deviations in spiking sequence. This may partially explain why cortical ripples in the semantic network do not display increases in BHA when they are coupled with SWR. In Khodagholy et al., cortical ripple oscillations were not prevalent in the rodent cortex outside of association areas[19]. Hence, it is also possible that cortical ripples that are detected in association areas are functionally different than cortical ripples in other areas. One possible explanation for this is the increased hippocampal-cortical and cortico-cortical connectivity in association cortices[64].

**Associations with theta oscillations**

Beyond ripple oscillations, theta oscillations have been described widely in the literature as another mechanism of hippocampal-cortical coordination during memory processes[65]. While SWRs mainly occur in non-theta states, evidence from rodent models suggests a relationship between theta and other high-frequency oscillations in the epsilon band in both the hippocampus[65–68] and neocortex[69]. Furthermore, a recent study investigating SWR in humans during NREM sleep described that cortical theta oscillations temporally precede SWRs in some regions and succeed them in others[23]. In our study, coincident hippocampal-ATL ripples were more likely to be associated with cortical theta oscillations in the ATL compared to non-coincident ripples, and for coincident ripples, theta oscillation peak succeeded the coincident ripple peak by 109ms. This is similar to the findings shown by Jiang et al.[23] where the temporal cortex demonstrated a high number of contacts demonstrating a theta-ripple relationship in humans during NREM sleep. This represents an interesting ruffle in the exploration of the mechanisms that underlie memory, as it is believed that theta oscillations underlie active memory function[65] while ripple oscillations represent offline memory function[1]. This points to the possibility that, in the awake human, these two mechanisms may function in concert such that cortical theta-ripple assemblies (even if temporally-asynchronous) may coordinate the precise reactivation of the ATL during word list retrieval. Alternatively, it is possible that concerted theta oscillations are underlying core encoding processes and coincident ripple oscillations function as an immediate

replay mechanism for heightened memory consolidation. In this case, it is possible that SWR which "successfully" co-occur with a cortical ripple may direct cortical theta oscillations, which more optimally engages the memory network as compared to isolated (or asynchronous) ripples. It is also possible that current approaches of detecting human SWRs[37] may, at least in part, detect epsilon oscillations, which would expected to be modulated by theta oscillations. However, that we only found co-ripple associated theta oscillations in the cortex and not the hippocampus would speak against this possibility.

### Conclusion

In conclusion, ripple oscillations serve as a dynamic mechanism underlying human memory function. In a word list learning task, we identify SWR-associated reactivation of specific cortical regions during free recall. There exists a unique interplay between the hippocampus and the ATL where, in times of SWR, the ATL exhibits synchronous cortical ripple and BHA increases. Coincident ripples across the hippocampus, ATL, and semantic areas show specificity in recall content and cortical region and may serve as a powerful mechanism for recruitment of semantic memory-containing regions. Further, coincident ripples between the hippocampus and the ATL are more likely to be associated with an ATL cortical theta oscillation. These findings extend our understanding of word memory retrieval, further elucidate the function of the ATL in coordinating activation of semantic processing regions, and provide evidence for coincident ripples as a mechanism of multi-nodal synchrony in human memory networks.

## Methods

### Subjects

Intracranial recordings were obtained from nine subjects (7 females), median age 32, age range 19-58) with medically intractable epilepsy undergoing iEEG recording at the Northwell Health (New York, USA) to assist in the identification of epileptogenic zones for potential surgical treatment. These subjects are continuously monitored with intracranial electrodes that were stereotactically placed, subdural grid or strip electrodes, or both, for a period of 1-3 weeks, during which they may participate in cognitive and functional testing. The decision to implant, location of implanted electrodes, and the duration of implantation were made entirely on clinical grounds by the treatment team. Subjects were selected to participate in this study based on presence of adequate hippocampal and cortical coverage and ability to perform a word list learning task. The study was conducted in accordance with the Institutional Review Board at the Feinstein Institutes for Medical Research (Northwell Health), and informed consent was obtained prior to testing.

No clinical seizures occurred during or within the two-hour period prior to the experimental blocks. All participants performed the task in their primary language (English or Spanish) and all participants were found to have left-hemisphere dominance for language identified via Wada testing and language fMRI. Patient information, including number of contacts, region of seizure focus, primary language, and post-implantation treatment are provided in Table 1.

### Stimuli and Task

Construction of word sets: In each trial, twelve monosyllabic English words were selected from a set of words such that they formed a set of three sentences of four syllables each (sentence trials) or a randomized word list (word list trials). Sentences had the same syntactic structure: noun + verb + adjective/descriptor + noun, but each individual word did not have any relation to other presented words (i.e. there was no syntactic dependence among words and subjects could not reasonably predict the upcoming word)[70]. Fifteen sentence trials and fifteen word list trials were randomly shuffled to create the thirty trials that composed the experiment. In each trial, the words were presented in an isochronous manner without any acoustic gap between them. Word stimulus onset

asynchrony (SOA) was 667ms (1.5 Hz word presentation) for all subjects except subjects 1 and 2 where the SOA was 500ms (2 Hz word presentation).

Subjects were provided with instructions for the task, including a sample set of words, and speaker volume was adjusted for comfort as needed. Each trial started with a subject-initiated push-button start, and participants waited 500ms before being presented with either a sentence trial or a word list trial. Upon the presentation of the words, participants waited 2000ms before being presented with a distractor task. For subject 3, immediately after the presentation of words, the participant was asked to recall as many words as they could in order to establish adequate comprehension of words. If the participant was unable to verbally recall any of the words from the presented set, the trial was manually aborted and the next trial began. If the participant was able to recall any words, the trial continued. Two out of thirty trials were manually aborted. In the arithmetic distractor task, participants were asked to determine whether a given arithmetic operation was true or false (e.g. “2+94=96” is true and “3+39=41” is false). The operation was visually presented one number or symbol at a time, each presented for 500ms with an inter-trial interval of 400ms. After the final number, subjects responded with a button press. In each trial, participants were presented two equations in succession. Following this, participants viewed a cue screen where they were asked to freely recall as many words as they could from the twelve words that were presented earlier in the trial. Participants pushed a button to designate that they were done recalling and were ready for the next set of words (in the next trial) to begin.

This task was executed using the Psychophysics Toolbox in MATLAB (MathWorks Inc., Natick, MA, USA). Visuals were presented using a 15” laptop or 24” monitor with sound stimuli sampled at 44.1k Hz. Sound stimuli were presented with a speaker located directly in front of the participant. To minimize distractions and external noise, all other electronic devices in the study room were switched off, the door was kept closed, and clinical staff were instructed to try to not enter or exit the room during the duration of the task.

### Identification of verbal recall events

A microphone affixed to a nearby stable surface recorded the entire experimental block, including the free recall periods for each trial. The onsets and offsets of each recall event and the contents of the recall were extracted in an offline analysis using Audacity auditory presentation software (Audacity, Oak Park, MI, USA). Recall events were designated as any relevant words that the patient stated, and any recall onset that occurred greater than 4 seconds after the offset of the previous recall event was marked as an independent event. Any trials induced by a mis-click or that included outside interference were removed from subsequent analysis.

To quantify the number of recalled words, we performed a median split by patient across all trials. Based on whether the patient was able to recall more than or less than than the median, each trial was marked as “effective” recall or “poor” recall, respectively. This aimed to normalize for variation in the number of recalled words per patient.

### Intracranial Recording Acquisition and Preprocessing

Intracranial recording sites were subdural grids, strips, stereo-EEG depth electrodes, or a combination thereof (Ad-Tech Medical Instrument Corp., Oak Creek, WI, USA; Integra LifeSciences, Princeton, NJ, USA; PMT Corp., Chanhassen, MN). Recording sites in the subdural grids and strips were 1- or 3-mm platinum disks with 4- or 10-mm intercontact (disk center to disk center) spacing. Recording sites in depth electrodes were 2-mm platinum cylinders with 0.8mm diameter and 4.4-mm intercontact spacing. During the recordings, the intracranial EEG signal was referenced to a subdermal electrode or subdural strip. Neural signals were acquired using a Tucker-Davis Technologies (TDT) PZ5M module (Tucker-Davis Technologies Inc., Alachua, FL) at either 1.5- or 3k Hz and saved for offline analysis. Prior to experimentation, signal quality and power spectra were

inspected online using TDT Synapse oscilloscope software, and if needed, changes were made to improve signal quality. During the task, artificial electrical pulses were created at the onset of each trial, onset of the distractor task, and onset of free recall cue for precise synchronization of data.

All data analysis was performed in MATLAB using FieldTrip[71] and custom written scripts. Data was resampled to 500 Hz and potential 60 Hz (and its 120 and 180 Hz harmonics) power-line noise was removed using a notch filter (zero-lag linear-phase Hamming-window FIR band-stop filter). Raw iEEG data was inspected visually to detect noisy or bad channels, which were excluded from further analysis. Data was average referenced to remove global artifacts. Seizure onset channels identified by the clinical team were excluded from analysis.

**Electrode Registration and Localization**

Prior to electrode implantation, a T1w structural MRI scan was collected for each patient. After electrode implantation, a CT scan were collected. We utilized the iELVis toolbox[72], which utilizes BioImage Suite[73], FreeSurfer[74], and custom written code for intracranial electrode localization. Briefly, electrode contacts were manually registered in the post-implantation CT scan using BioImage Suite, which is co-registered to the pre-implantation MRI scan in an attempt to minimize localization error due to brain shift. FreeSurfer is implemented to align the patient's pre-implantation MRI to a standard coordinate space, segment the cortical surface, assign anatomical locations for each contact, and determine hippocampal subfields in each patient. Finally, iELVis software is used to project the contact locations onto FreeSurfer's standard surface. For all anatomical regions of interest analysis, Freesurfer parcellation was implemented to identify contacts of interest, and the location of these contacts on the subject brain were implemented for confirmation.

**Selection of Semantic Network Contacts**

Electrode responsiveness was selected by contacts where HFA during the word presentation window was significantly increased. We followed the methodology implemented by Fedorenko et al. in a previous study[31]. Sentence-responsive contacts were identified as contacts in which the magnitude of HFA was significantly higher for trials of the sentence condition than the word list condition; word list-responsive contacts were identified in which the activity was opposite. To identify the functionality and specificity in responsiveness across contacts, a 500 ms epoch of HFA was constructed for each presented word, with the epoch beginning at the onset of each presented word and ending 50ms prior to the onset of the next word, and each epoch was classified as being part of a sentence trial or a word list trial. For each trial, a pre-trial baseline of equal duration (450ms) was also identified and the HFA signal was similarly constructed. The signal was then baseline corrected using this pre-trial baseline. For each electrode, we then computed the mean HFA across the twelve word positions in each trial for each condition. We then correlated the trial means with a vector of condition labels (sentences = 1; word lists = -1). A resulting Spearman's rho ws then computed and provided a benchmark which to test the significance of correlations. A permutation distribution was constructed by randomly reordering the condition labels and calculating a new Spearman's rho for each iteration. This process was repeated 1000 times. Correlations that were in the top or bottom 2.5% of the distribution were denoted as significant. Significant contacts with a positive rho value (that is, a positive correlation) were marked as sentence-responsive, and significant contacts with a negative rho value were marked as word list-responsive. Hence, the semantic network was divided into contacts that were preferentially sentence-responsive and contacts that were preferentially responsive to non-sentence trials. Separately, contacts that showed increases in HFA for both sentence and word list trials as compared to baseline were marked as general language-responsive.

We also identified contacts that were in the anterior temporal lobe. To systematically define these contacts, we identified the axis between the most anterior tip of the temporal lobe to the most posterior aspect of the middle temporal lobe as defined by the Desikan-Killiany atlas[75] overlaid onto

each subject's specific brain image. All contacts that were anterior to the orthogonal line constructed at one-third of the constructed temporal lobe axis were defined as being in the ATL.

### High-frequency broadband signal and related spectral analysis

High frequency activity (HFA) signal was defined as the mean normalized power of 70-150 Hz. For analyses in which spectrograms were computed or HFA activity was compared between contact types, HFA power was computed independently for each contact by: (1) bandpass filtering the iEEG signal in 10 Hz bands (i.e. 70-80 Hz, 80-90 Hz, 90-100 Hz, and so on, but excluding windows of 118-122 Hz to exclude potential power line noise) using a fourth-order Butterworth filter; (2) applying a Hilbert transform to each individual frequency band and taking the absolute value of the resulting envelope; (3) amplitude normalization, via division of the mean of the frequency band signal; (4) averaging all normalized frequency band envelopes. This procedure results in a single time series that serves as a proxy for mean neuronal activity at a given contact. This normalization procedure has been implemented previously[8,76] and corrects for the 1/f decay in EEG power spectra while providing temporal smoothing at the higher frequencies. Prior to any analysis implementing this derived HFA signal, the data was visually inspected for artifacts. Candidate artifacts were identified as peaks 4 standard deviations above the mean HFA signal across contacts. Artifacts were then visually inspected, and if needed, contacts were marked to be excluded from any additional analysis.

Epochs of HFA signal were created as needed for time periods of interest, including ripple-locked, response time-locked, and word presentation-locked. For each, the HFA signal was baseline-normalized with a pre-event baseline (typically the 500ms pre-trial baseline or the 500ms period immediately after response cue). This allowed for the comparison of contacts within regions of interest across subjects. To compare HFA across two signals of interest, a two-tail nonparametric cluster-based test (clustering across time bins) was implemented using the fieldtrip toolbox[71]. For single-electrode examples, due to smaller sample sizes, a two-tail Wilcoxon signed-rank test was implemented.

To examine the effect size of HFA effects, we implemented Cohen's d. We evaluated the effect size as the following: small (d=0.2), medium (d=0.5), and large (d=0.8)[77]. We implemented this metric when determining the magnitude of effect, by electrode, for (1) preferred and non-preferred analysis (averaging over a 500ms epoch around SWR peak for each) and (2) examining peri-SWR HFA compared to baseline (comparing 500ms epoch around SWR peak with a 500ms period preceding this).

### Ripple Detection

Ripple detection was performed offline. For SWR detection, we identified an electrode contact located in or adjacent to the lateral aspect of the body of the hippocampus (CA1/CA2 subfield region). The exact anatomical location of electrode selection in each patient is depicted in Figure S1. The signal was referenced to the closest nearby white matter contact, 8.8mm away from the selected hippocampal contact and filtered between 70 and 180 Hz using a zero-lag, linear-phase Hanning window FIR filter with 5 Hz transition band. A Hilbert transform was then applied to attain signal amplitude. As in[78], this signal was clipped to 3 standard deviations to minimize bias that may arise from high ripple rates. The clipped signal was then squared and smoothed via a Kaiser-window FIR low-pass filter with 40 Hz cutoff. To attain a baseline for event detection, the mean and standard deviation of the pre-experiment resting period signal was used after removal of 100ms periods surrounding any manually-detected IEDs (please see below for methodology and rationale). Events from the original signal that exceeded 3 standard deviations above baseline were selected as candidate SWR events. Onset and offset of each event was defined as the timepoints where the ripple band power decreased below 2 standard deviations. Events shorter than 42ms (computed as the duration of 3 cycles of 70 Hz) and longer than 250ms were removed. Events where the peak-to-

peak difference was under 200ms of one another were merged. SWR peak was then aligned to the maximum amplitude of the ripple-band envelope.

To control for global and transient artifacts, a control detection was performed on the common average signal of all contacts. Any SWR events that occurred within 50ms of a common average ripple-band peak were removed. Further, to avoid inclusion of any pathological high-frequency discharges, specifically inter-ictal discharges (IEDs) a manual detection process was used. Candidate IEDs were identified as having an amplitude greater than 4 standard deviations above mean, and a peak width of less than 100ms. Of these candidates, true IEDs were manually selected based on patient-specific IED physiology. Following this, an automatic IED detection method was also implemented; the raw hippocampal bipolar LFP was filtered between 25-60 Hz (using a zero-lag, linear-phase Hamming window FIR filter) and a similar methodology to the ripples analysis above was applied (rectifying, squaring, normalizing). Detected events that exceeded 5 standard deviations were marked as IEDs. SWR events occurring within 200ms of an IED event were rejected[79]. For identification of cortical ripples, this same ripple detection algorithm was implemented. To confirm that all detected SWR and ripple events were oscillations, we implemented the eBOSC toolbox[80,81] to confirm that all identified events had at least one oscillatory cycle within the ripple frequency range. This procedure was also executed for all cortical contacts analyzed, including ATL and semantic network contacts.

We primarily assessed SWR in two main conditions: (a) perception of word list, during which participants listened to the word list and (b) recall, in which four-second windows around the onset of independent verbal recall events (defined as verbal recall events that were at least four seconds apart) were determined. This aimed to maximize the potential that SWR events were directly involved in the retrieval and recall process. SWR events that coincided with other parts of the task (i.e. perception of word list or distractor task) were removed from this set of SWR events.

Human SWR have been proposed to predominantly occur in the 80-140 Hz frequency range and most studies utilized an 80-150 Hz frequency range for SWR detection[37]. However, we aimed to minimize the possibility of filtering out ripple events, and hence, a wider frequency range of 70-180 Hz was used (similar to previous studies[8,12,37]). Demonstration of the peak ripple frequencies show that most ripples were indeed within the 80-140 Hz range (Figure 1F).

**Spectral analysis and detection of aperiodic oscillatory activity**

We then evaluated whether the increases in SWR-associated ATL HFA were simply increases in broadband HFA or cortical ripples. As ripples are rhythmic phenomena, if cortical ripples were indeed driving this effect, we would expect to identify an increase in oscillations detected within the ripple-band. Per prior studies, we expect the cortical ripples to have a peak frequency within the 80-120 Hz range[9,15–17]. We performed a wavelet-based frequency analysis for the 10-200 Hz frequency range (in 1-Hz steps; width 8 Hz) for each detected ATL cortical ripple. We removed 3 Hz bands around 60, 120, and 180 Hz to remove line noise. We then separated all ATL cortical ripples that occurred within 100ms of a hippocampal SWR and compared the log-frequency spectrograms for cortical ripples that were coincident with a SWR and isolated cortical ripples without coincident SWR. A cluster-based permutation test was implemented to determine significant frequency clusters.

To more closely assess the relationship between ATL cortical ripples and low-frequency oscillatory phenomena, we performed a wavelet-based frequency analysis for the 1-12 Hz frequency range (in 0.1 Hz steps; width 6 Hz) for each detected ATL cortical ripple. To visualize the changes in lower frequencies, we constructed plots depicting log-power as a function of frequency (averaging over a 500ms window around cortical ripple peak) and power as a function of time. We separated these plots between coincident and non-coincident ATL cortical ripples to assess for differences between the two. We confirmed these findings by implementing the FOOOF algorithm (version 1.0.0)[42], which

assists in the decomposition of a neural signal into a periodic and aperiodic component on the single-trial level. We detected low-frequency oscillations in the 2-10 Hz range on peri-SWR data (400ms epoch). The minimum peak height was selected to be 0.3 and the peak width limits were set to be 1-12 Hz. The resulting identified peaks were then plotted onto a histogram to depict most prominent SWR-associated low frequency oscillations.

### Detection of theta oscillations

Theta oscillation detection was performed similar to prior studies[23,82]. A zero-phase shift 4-8 Hz bandpass filter was applied to the single-channel (cortical contact) LFP data. A channel-specific cutoff was set at 3 standard deviations above the mean and was applied to each channel's Hilbert envelope to identify peaks of theta oscillations. The start and stop of each theta oscillation event was determined when the power dropped below 1 standard deviation above the channel mean. Theta bursts were included for analysis if their durations fell within 375 and 1000ms (defined as 3 cycles of 8 Hz and 3 Hz, respectively).

### Peri-event time histograms

To construct peri-event time histograms across experimental conditions, we used a bin width advised by Scott's optimization method, which optimizes bin size to event density[83]. For PETH locked to sentence onset, we assessed all ripples in the -0.5 to 10 second window relative to onset of word list presentation and utilized an optimized bin size of 200ms with 7-point smoothing. To determine significant time bins, 5000 iterations of peri-presentation onset time histograms were computed by circularly jittering ripple times across the two-second pre-word list presentation window. This enabled us to maintain statistical power despite a low number of ripple events. A permutation test was performed to determine significant time windows. Time windows that were in the top or bottom 2.5% of the distribution (thus implementing an alpha-value of 0.05) were denoted as significant. A similar approach was taken for the peri-verbal recall PETH, but here, statistical power was computed by circularly jittering ripple times 5000 times across the same -4 to 1 second window relative to onset of verbal free recall (while implementing 90ms bin size with 7-point smoothing). Finally, to compare PETH around the onset of effective vs poor recall periods, we assessed the same -4 to 1 second window with identical 230ms and 4-point smoothing for the two PETH. To determine significance, we shuffled labels of effective and poor recall and generated a distribution of mean SWR rate differences (5000 iterations). This generated a distribution by which we identified significant timebins.

### Cross-correlograms

To examine "co-rippling" between two brain regions, we used the ripple peak time index to produce cross-correlograms. For each cortical electrode, we computed a cross-correlation between detected cortical ripples and SWR. We pooled these cross-correlations across trials for each electrode pair in each participant, which creates a single cross-correlogram for each pair of contacts. We normalized the amplitude of each cross-correlation by the duration of the time window of interest and number of electrode pairs such that values represented coincidences per second. For this analysis, we implemented 10ms bins. To determine significance of synchronous ripple events, we jittered cortical ripple event timing and constructed a new cross-correlogram. This procedure was repeated 5000 times and implemented as a distribution for a permutation test. This procedure was applied separately for ATL contacts and semantic network contacts.

### Temporal resolution of coincident ripple events

To determine the temporal resolution of co-ripple events relative to verbal recall onset, we implemented proportions to normalize for the increase in SWR events that occurs prior to verbal free recall. That is, instead of quantifying the rate of coincident ripple events, we quantified the chance that a SWR event was coincident with a coincident ATL cortical ripple event prior to verbal free recall. A coincident ripple event was defined as two ripple events where the peak-to-peak duration was less than 100ms (defined as half of the 200ms maximum ripple duration), as the peak of ripple events are

more readily detectable compared to the onset/offset (which differs depending on manually-defined thresholds). We constructed a PETH for the -4 to 2 second window relative to verbal recall onset implementing 300ms bins with 8-point smoothing. To determine significance across timebins, we jittered cortical ripple event timing and constructed a new PETH. This procedure was repeated 5000 times and implemented as a distribution for a permutation test.

## Acknowledgements

We would like to thank the subjects for volunteering their time and effort to participate in our study. We also thank the Epilepsy Monitoring Unit staff at the North Shore University Hospital for their support throughout the study. We thank Yitzhak Norman and Jose Herrero for providing helpful feedback on the analysis and methods.

## References

1. Buzsáki, G. Hippocampal sharp wave-ripple: A cognitive biomarker for episodic memory and planning. *Hippocampus* **25**, 1073–1188 (2015).
2. Buzsáki, G. Hippocampal sharp waves: Their origin and significance. *Brain Res.* **398**, 242–252 (1986).
3. Joo, H. R. & Frank, L. M. The hippocampal sharp wave–ripple in memory retrieval for immediate use and consolidation. *Nat. Rev. Neurosci.* **19**, 744–757 (2018).
4. Klinzing, J. G., Niethard, N. & Born, J. Mechanisms of systems memory consolidation during sleep. *Nat. Neurosci.* **22**, 1598–1610 (**20**19).
5. Helfrich, R. F. *et al.* Bidirectional prefrontal-hippocampal dynamics organize information transfer during sleep in humans. *Nat Commun* **10**, 3572 (2019).
6. Ngo, H.-V., Fell, J. & Staresina, B. Sleep spindles mediate hippocampal-neocortical coupling during long-duration ripples. *eLife* **9**, e57011 (2020).
7. Norman, Y., Raccah, O., Liu, S., Parvizi, J. & Malach, R. Hippocampal ripples and their coordinated dialogue with the default mode network during recent and remote recollection. *Neuron* **109**, 2767-27**8**0.e5 (2021).
8. Norman, Y. et al. Hippocampal sharp-wave ripples linked to visual episodic recollection in humans. *Science* **365**, eaax10**30** (2019).
9. Vaz, A. P., Inati, S. K., Brunel, N. & Zaghloul, K. A. Coupled ripple oscillations between the medial temporal lobe and neocortex retrieve human memory. Science **363**, 975–978 (2019).
10. Zhang, H., Fell, J. & Axmacher, N. Electrophysiological mechanisms of human memory consolidation. *Nat. Commun.* **9**, 4103 (2018).
11. Sakon, J. J. & Kahana, M. J. Hippocampal ripples signal contextually mediated episodic recall. *Proc National Acad Sci* **119**, e2201657119 (2022).
12. Skelin, I. et al. Coupling between slow waves and sharp-wave ripples engages distributed neural activity during sleep in humans. *Proc. Natl. Acad. Sci.* **118**, e20**120**75118 (2021).
13. Tong, A. P. S., Vaz, A. P., Wittig, J. H., Inati, S. K. & Zaghloul, K. A. Ripples reflect a spectrum of synchronous spiking activity in human anterior temporal lobe. eLife 10, e68401 (2021).
14. Kucewicz, M. T. et al. High frequency oscillations are associated with cognitive processing in human recognition memory. *Brain* **137**, 2231–2244 (2014).
15. Dickey, C. W. et al. Widespread ripples synchronize human cortical activity during sleep, waking, and memory recall. Proc. Natl. Acad. Sci. **119**, e2**107**797119 (2022).
16. Verzhbinsky, I. A. et al. Co-occurring ripple oscillations facilitate neuronal interactions between

cortical locations in humans. *bioRxiv* 2023.05.20.541588 (2023) doi:10.1101/2023.05.20.541588.
17. Silva, M. et al. Neocortico-hippocampal ripple-based coordination during naturalistic encoding. bioRxiv 2023.09.27.559739 (2023) doi:10.1101/2023.09.27.559739.
18. Arnulfo, G. et al. Long-range phase synchronization of high-frequency oscillations in human cortex. Nat. Commun. 11, 5363 (2020).
19. Khodagholy, D., Gelinas, J. N. & Buzsáki, G. Learning-enhanced coupling between ripple oscillations in association cortices and hippocampus. Science **358**, 369–372 (2017).
20. Miller, K. J. Broadband Spectral Change: Evidence for a Macroscale Correlate of Population Firing Rate?: Figure 1. *J. Neurosci.* **30**, 6477–6479 (2010).
21. Ray, S. & Maunsell, J. H. R. Different Origins of Gamma Rhythm and High-Gamma Activity in Macaque Visual Cortex. *PLoS Biol.* **9**, e**100**0610 (2011).
22. Ray, S., Crone, N. E., Niebur, E., Franaszczuk, P. J. & Hsiao, S. S. Neural Correlates of High-Gamma Oscillations (60–200 Hz) in Macaque Local Field Potentials and Their Potential Implications in Electrocorticography. J. Neurosci. **28**, 11526–11536 (2008).
23. Jiang, X., Gonzalez-Martinez, J. & Halgren, E. Coordination of Human Hippocampal Sharpwave Ripples during NREM Sleep with Cortical Theta Bursts, Spindles, Downstates, and Upstates. *J Neurosci* **39**, 87**44**–8761 (2019).
24. Friederici, A. D. & Gierhan, S. M. The language network. *Curr. Opin. Neurobiol.* **23**, 250–254 (2013).
25. Fedorenko, E. & Thompson-Schill, S. L. Reworking the language network. *Trends Cogn. Sci.* **18**, 120–126 (2014).
26. Murphy, E. et al. The spatiotemporal dynamics of semantic integration in the human brain. Nat. Commun. 14, 6**33**6 (2023).
27. Woolnough, O. et al. Spatiotemporally distributed frontotemporal networks for sentence reading. Proc National Acad Sci 120, e2300252120 (2023).
28. Zhu, Y. et al. Distinct spatiotemporal patterns of syntactic and semantic processing in human inferior frontal gyrus. *Nat. Hum. Behav.* **6**, 1104–1111 (2022).
29. Forseth, K. J. et al. A lexical semantic hub for heteromodal naming in middle fusiform gyrus. Brain **141**, 2112–2126 (2018).
30. Ruff, I., Blumstein, S. E., Myers, E. B. & Hutchison, E. Recruitment of anterior and posterior structures in lexical–semantic processing: An fMRI study comparing implicit and explicit tasks. *Brain Lang.* **105**, 41–49 (2008).
31. Fedorenko, E. et al. Neural correlate of the construction of sentence meaning. Proc National Acad Sci **113**, E6256–E6262 (2016).
32. Guo, C. C. et al. Anterior temporal lobe degeneration produces widespread network-driven dysfunction. Brain **136**, 2979–2991 (2013).
33. Herlin, B., Navarro, V. & Dupont, S. The temporal pole: From anatomy to function—A literature appraisal. *J. Chem. Neuroanat.* **113**, 101925 (2021).
34. Friederici, A. D., Wang, Y., Herrmann, C. S., Maess, B. & Oertel, U. Localization of early syntactic processes in frontal and temporal cortical areas: A magnetoencephalographic study. *Hum. Brain Mapp.* **11**, 1–11 (2000).
35. Humphries, C., Love, T., Swinney, D. & Hickok, G. Response of anterior temporal cortex to syntactic and prosodic manipulations during sentence processing. Hum. Brain Mapp. **26**, 128–1**38** (2005).
36. Poeppel, D. & Hickok, G. Towards a new functional anatomy of language. *Cognition* **92**, 1–12

(2004).
37. Liu, A. A. et al. A consensus statement on detection of hippocampal sharp wave ripples and differentiation from other fast oscillations. Nat. Commun. 13, 6000 (2022).
38. Jiang, X. et al. Improved identification and differentiation from epileptiform activity of human hippocampal sharp wave ripples during NREM sleep. *Hippocampus* **30**, 610–622 (2020).
39. Chen, Y. Y. et al. Stability of ripple events during task engagement in human hippocampus. *Cell Rep.* **35**, 109304 (2021).
40. Vaz, A. P., WittigJr., J. H., Inati, S. K. & Zaghloul, K. A. Replay of cortical spiking sequences during human memory retrieval. Science **367**, 1131–1134 (2020).
41. Leszczyński, M. et al. Dissociation of broadband high-frequency activity and neuronal firing in the neocortex. *Sci. Adv.* **6**, eabb0977 (2020).
42. Donoghue, T. et al. Parameterizing neural power spectra into periodic and aperiodic components. *Nat. Neurosci.* **23**, 1655–1665 (2020).
43. Sakon, J. J., Halpern, D. J., Schonhaut, D. R. & Kahana, M. J. Human Hippocampal Ripples Signal Encoding of Episodic Memories. J. Neurosci. 44, e0111232023 (2024).
44. Henin, S. et al. Spatiotemporal dynamics between interictal epileptiform discharges and ripples during associative memory processing. Brain **144**, 1590–1602 (2021).
45. Rothschild, G., Eban, E. & Frank, L. M. A cortical–hippocampal–cortical loop of information processing during memory consolidation. Nat. Neurosci. 20, 251–259 (2017).
46. Logothetis, N. K. et al. Hippocampal–cortical interaction during periods of subcortical silence. *Nature* **491**, 547–553 (2012).
47. Nitzan, N., Swanson, R., Schmitz, D. & Buzsáki, G. Brain-wide interactions during hippocampal sharp wave ripples. Proc. Natl. Acad. Sci. 119, e2200931119 (2022).
48. Abadchi, J. K. et al. Spatiotemporal patterns of neocortical activity around hippocampal sharp-wave ripples. eLife 9, e51972 (2020).
49. Zhang, H. et al. Awake ripples enhance emotional memory encoding in the human brain. Nat. Commun. 15, 215 (2024).
50. Mukamel, R. et al. Coupling Between Neuronal Firing, Field Potentials, and fMRI in Human Auditory Cortex. Science **309**, 951–954 (2005).
51. Miller, K. J. et al. Broadband changes in the cortical surface potential track activation of functionally diverse neuronal populations. *NeuroImage* **85**, 711–720 (2014).
52. Todorova, R. & Zugaro, M. Hippocampal ripples as a mode of communication with cortical and subcortical areas. Hippocampus 30, 39–49 (2020).
53. Sirota, A., Csicsvari, J., Buhl, D. & Buzsáki, G. Communication between neocortex and hippocampus during sleep in rodents. Proc. Natl. Acad. Sci. 100, **206**5–2069 (2003).
54. Mollo, G., Cornelissen, P. L., Millman, R. E., Ellis, A. W. & Jefferies, E. Oscillatory Dynamics Supporting Semantic Cognition: MEG Evidence for the Contribution of the Anterior Temporal Lobe Hub and Modality-Specific Spokes. *PLoS ONE* **12**, e0169269 (2017).
55. Ralph, M. A. L., Sage, K., Jones, R. W. & Mayberry, E. J. Coherent concepts are computed in the anterior temporal lobes. Proc. Natl. Acad. Sci. 107, 2717–2722 (2010).
56. Binder, D. K., Rau, G. & Starra, P. A. Hemorrhagic Complications of Microelectrode-Guided Deep Brain Stimulation. *Stereotactic and Functional Neurosurgery* **80**, 28–**31** (2003).
57. Sabsevitz, D. S. et al. Use of preoperative functional neuroimaging to predict language deficits from epilepsy surgery. *Neurology* **60**, 1788–1792 (2003).
58. Snyder, K. M. et al. Critical role of the ventral temporal lobe in naming. *Epilepsia* **64**, 1200–1213

(2023).
59. Patel, J., Schomburg, E. W., Berényi, A., Fujisawa, S. & Buzsáki, G. Local Generation and Propagation of Ripples along the Septotemporal Axis of the Hippocampus. J. Neurosci. 33, 17029–17041 (2013).
60. Jeneson, A., Mauldin, K. N., Hopkins, R. O. & Squire, L. R. The role of the hippocampus in retaining relational information across short delays: The importance of memory load. *Learn. Mem.* **18**, 301–305 (2011).
61. Fernández-Ruiz, A. et al. Long-duration hippocampal sharp wave ripples improve memory. Science **364**, 1082–1086 (2019).
**62**. Filippo, R. D. & Schmitz, D. Differential ripple propagation along the hippocampal longitudinal axis. eLife 12, e85488 (2023).
63. Vaz, A. P., Wittig, J. H., Inati, S. K. & Zaghloul, K. A. Backbone spiking sequence as a basis for preplay, replay, and default states in human cortex. Nat. Commun. 14, 4723 (2023).
64. Schmahmann, J. D. et al. Association fibre pathways of the brain: parallel observations from diffusion spectrum imaging and autoradiography. Brain **130**, 630–653 (2007).
65. Herweg, N. A., Solomon, E. A. & Kahana, M. J. Theta Oscillations in Human Memory. *Trends Cogn Sci* **24**, 208–227 (2020).
66. Tort, A. B. L. et al. Dynamic cross-frequency couplings of local field potential oscillations in rat striatum and hippocampus during performance of a T-maze task. Proc. Natl. Acad. Sci. 105, 20517–20522 (2008).
67. Scheffer-Teixeira, R. et al. Theta Phase Modulates Multiple Layer-Specific Oscillations in the CA1 Region. *Cereb. Cortex* **22**, 2404–2414 (2012).
68. Tort, A. B. L., Scheffer-Teixeira, R., Souza, B. C., Draguhn, A. & Brankačk, J. Theta-associated high-frequency oscillations (110–160Hz) in the hippocampus and neocortex. *Prog. Neurobiol.* **100**, 1–14 (2013).
69. Canolty, R. T. et al. High Gamma Power Is Phase-Locked to Theta Oscillations in Human Neocortex. Science **313**, 1626–1628 (2006).
70. Kollmeier, B. et al. The multilingual matrix test: Principles, applications, and comparison across languages: A review. *Int. J. Audiol.* **54**, 3–16 (2015).
71. Oostenveld, R., Fries, P., Maris, E. & Schoffelen, J.-M. FieldTrip: Open Source Software for Advanced Analysis of MEG, EEG, and Invasive Electrophysiological Data. *Comput. Intell. Neurosci.* **2011**, 156869 (2011).
72. Groppe, D. M. et al. iELVis: An open source MATLAB toolbox for localizing and visualizing human intracranial electrode data. *Journal of Neuroscience Methods* **281**, 40–48 (2017).
73. Papademetris, X. et al. BioImage Suite: An integrated medical image analysis suite: An update. *insight J.* **2006**, 209 (2006).
74. Fischl, B. FreeSurfer. NeuroImage 62, 774–781 (2012).
75. Desikan, R. S. et al. An automated labeling system for subdividing the human cerebral cortex on MRI scans into gyral based regions of interest. NeuroImage 31, 968–980 (2006).
76. Norman, Y., Yeagle, E. M., Harel, M., Mehta, A. D. & Malach, R. Neuronal baseline shifts underlying boundary setting during free recall. Nat Commun 8, 1301 (2017).
77. Cohen, J. *Statistical Power Analysis for the Behavioral Sciences*. (2013).
78. Stark, E. et al. Pyramidal Cell-Interneuron Interactions Underlie Hippocampal Ripple Oscillations. Neuron **83**, 467–480 (2014).
79. Gelinas, J. N., Khodagholy, D., Thesen, T., Devinsky, O. & Buzsáki, G. Interictal epileptiform

discharges induce hippocampal–cortical coupling in temporal lobe epilepsy. *Nat. Med.* **22**, 641–648 (2016).
80. Whitten, T. A., Hughes, A. M., Dickson, C. T. & Caplan, J. B. A better oscillation detection method robustly extracts EEG rhythms across brain state changes: The human alpha rhythm as a test case. NeuroImage 54, 860–874 (2011).
81. Kosciessa, J. Q., Grandy, T. H., Garrett, D. D. & Werkle-Bergner, M. Single-trial characterization of neural rhythms: Potential and challenges. NeuroImage 206, 116331 (2020).
82. Gonzalez, C. E. et al. Theta Bursts Precede, and Spindles Follow, Cortical and Thalamic Downstates in Human NREM Sleep. J Neurosci 38, 9989–10001 (2018).
83. Scott, D. W. On optimal and data-based histograms. *Biometrika* **66**, 605–610 (1979).